Dynamic Modeling and Optimization of Permanent Magnet Synchronous Electrical Machine Propulsion Powertrain at Different Modeling Levels

Abdullah Waheeb Jaffer Omer Ghareeb[1], Aminu Babangida[2]* and Péter Tamás Szemes[2]

[1]Department of Electrical Engineering and Mechatronics, Vehicles and Mechatronics Institute, Faculty of Engineering, University of Debrecen, Ótemető u. 2-4, H-4028 Debrecen, Hungary, abdullahwaheeb@mailbox.unideb.hu

[2]Department of Vehicles Engineering, Vehicles and Mechatronics Institute, Faculty of Engineering, University of Debrecen, Ótemető u. 2-4, H-4028 Debrecen, Hungary, szemespeter@eng.unideb.hu

*Correspondence: aminu.babangida@eng.unideb.hu

Abstract: Electric vehicles (EVs) have emerged as a compelling solution to mitigate environmental concerns and meet the growing demand for energy-efficient transportation systems. The careful selection of the electric motor is critical in determining the overall performance of the EV. This paper uses an EV from the University of Debrecen as a reference to comprehensively study the feasibility of using a permanent magnet brushless direct current (PMBLDC) motor in the vehicle. The optimal performance of the overall powertrain is realized based on a proportional integral and derivative (PID) controller. The advanced nonlinear dynamics of the system make the performance of the control algorithm unrealistic. The PID is optimized based on a genetic algorithm (GA-PID) to address this limitation and achieve optimal performance. The integral performance indices are used as a fitness value for the optimization problem. However, MATLAB/Simulink/Simscape is used to comprehensively investigate and compare the simplified and advanced models of a three-phase, four-pole, Y-connected PMBLDC motor in the EV application. The simulation results indicate that the proposed electrical machine is promising in EVs, achieving 90.90 % energy efficiency, thereby decreasing the energy consumption by 11.12 % compared to the measured real-world results. This research contributes significantly to energy efficiency, power efficiency, and thermal performance, offering invaluable insights into the optimal selection and modeling of PMBLDC motors at varying complexity levels in EVs. Ultimately, this study steers the industry towards a more sustainable and environmentally conscious trajectory.

Keywords: Advanced Powertrain; EVs; Genetic Algorithm; PID; PMBLDC Motor

1 Introduction

The car industry is experiencing a fundamental transformation toward electrification to alleviate greenhouse gas emissions and reliance on gas-powered vehicles; with their promise of cleaner and more energy-efficient mobility, EVs have become a well-known answer [1]. The electric motor that propels an EV is crucial to its performance. PMBLDC motors, one of the many types of motors, have drawn attention due to their compact design, high efficiency, and reliability [2]. This research explores mechatronics engineering to answer two key questions: Which model of a three-phase PMBLDC motor is best suited for integration into an electric vehicle, and how can its performance be enhanced to satisfy the particular requirements of this application? We acknowledge that, despite simplified models being frequently used for their computational effectiveness, complicated models provide a higher level of accuracy in describing the behavior of the motor. Therefore, the overall goals of this research paper are summarised as follows: First, comprehensive research on the theoretical technology of PMBLDC motors and their suitability for EV applications, considering the benefits and unique features. It also compares motor models at different advancedity levels, such as the simplified and advanced models. Moreover, the required adjustments for the selected models are performed to meet the electric vehicle's requirements, such as maximizing system's efficiency.

Several works have been put forward in the field of PMBLDC motors for EV applications in recent years. In [3], an EV powered by PMBLDC motor and the corresponding impact on the state of ripples and charge in the DC voltage at the battery power was evaluated in MATLAB software. In [4], a 5 kW, 48 V rated PMBLD motor was proposed using MATLAB/Simulink environment for the speed control of an EV during the vehicle's acceleration and deceleration, taking error into consideration as the critical factor. A proportional-integral (PI) and adaptive neuro-fuzzy inference system (ANFIS) controllers were used to reduce the error. The study in [5] proposed a tilt integral derivative (TID) controller to regulate the speed of the PMBLDC motor, thereby optimizing the motor torque and speed to enhance its control in real-time for efficient performance in EV applications. In [6], the pole of the PMBLDC was designed for EV application. The research evaluated the essential role of the pole count of the PMBLDC motor in optimizing its performance in EVs. The study in [7] highlights the analysis and design of two and three-wheeler electric vehicle motor drives using PMBLDC motor rated at 1.5 kW, 3000 rpm, and 120 V. In [8], PI-based particle swarm optimization (PSO-PI) was proposed to control the speed of the motor for efficient energy consumption in EV, reducing the energy consumption by 3.1%.

Moreover, in [9], the equivalent power circuit and operation principle of an EV powered by a three-phase PMBLDC motor was investigated on the basis of regenerative braking technology. In [10], a PMBLDC motor drive system was designed based on intelligent controllers to evaluate its performance in the field of

EVs. The time-dependent profile of the motor shaft's reflected torque and speed variables was determined and used as reference data for the proposed controllers.

Inspired by the above, this research proposes an optimal design of an electric Crafter (e-Crafter) powered by a PMBLDC electrical machine with reference to the real EV of the faculty of engineering based on the enhanced GA-PID control algorithm. This research leverages the models of the electrical machine at different levels of advancedity, considering the technical differences between the two. The main contributions of this paper are as follows:

1) For the first time, this study proposes two levels of a modeling approach for the PMBLDC motor that would be suitable for electric vehicle applications, taking into account the complexity levels and technical differences.
2) For the first time, this article presents the optimization of the VW e-Crafter (pure electric) powertrain-based PMBLDC electrical machine using the GA technique.
3) In this article, the simplified and advanced models of the electrical machine are applied to the VW Crafter electric vehicle as an extended version of our conference paper [11] to study optimal speed-tracking performance and energy consumption.
4) A recent study in [8] proposed a PMBLDC motor and reduced energy consumption by 3.1%. In this article, a 90.90% energy efficiency has been achieved, thereby decreasing the energy consumption by 11.12% compared to the measured real-world results.

2 Mathematical Modeling

The advanced model takes into account the detailed three-phase model with control, energy source, power electronics, and the motor itself. In contrast, the simplified model considers the energy source, control, and the motor itself at an abstraction level. Mathematically, the behavior of the motor is modeled in terms of its voltage, back EMF, speed, and torque. Therefore, this section presents the mathematical model of the advanced and simplified models of the PMBLDC motor.

2.1 Advanced Model

The mathematical model of the electric motor, which contains both mechanical and electrical components, can be represented by a matrix. The three-phase currents, I [A], three-phase voltages,V [Volts], and three-phase back EMFs, E [Volts] are all included in this model. The equations that control the behavior of the motor are expressed as in [12] as follows:

$$\begin{pmatrix} V_a \\ V_b \\ V_c \end{pmatrix} = R \begin{pmatrix} i_a \\ i_b \\ i_c \end{pmatrix} (L - M) \frac{d}{dt} \begin{pmatrix} i_a \\ i_b \\ i_c \end{pmatrix} + \begin{pmatrix} E_a \\ E_b \\ E_c \end{pmatrix} \quad (1)$$

$$\begin{pmatrix} E_a \\ E_b \\ E_c \end{pmatrix} = K_e \omega_m \begin{pmatrix} F(\theta_e) \\ F\left(\theta_e - \frac{2\pi}{3}\right) \\ F\left(\theta_e + \frac{2\pi}{3}\right) \end{pmatrix} \quad (2)$$

Where ω_m[rpm] and θ_e are the rotor mechanical speed and electrical angle, respectively. The electromagnetic torque, T_e [Nm] is expressed as in [12] as follows:

$$T_e = K_t \begin{pmatrix} i_a \\ i_b \\ i_c \end{pmatrix} \begin{pmatrix} F(\theta_e) \\ F\left(\theta_e - \frac{2\pi}{3}\right) \\ F\left(\theta_e + \frac{2\pi}{3}\right) \end{pmatrix} \quad (3)$$

$$T_e = J \frac{d\omega_m}{dt} + B\omega_m + T_l \quad (4)$$

Where R is the resistance matrix, L [H] is inductance matrix, M [H] is mutual inductance between the phases, K_e [V-s/rad] is the back EMF constant, K_t [Nm/A] torque constant, J [kgm^2] is the rotor moment of inertia, T_l [Nm] is load torque, $F(\theta_e)$ is the back EMF function of the position of the rotor [12].

2.2 Simplified Model

The simplified motor model used is presented in Figure 1, considering speed and torque envelopes. As a result, we only looked at the outer loop of the more straightforward equivalent PMBLDC Model, which uses a PI control technique to control the motor speed due to its simple structure and easy implementation [13].

The transfer function from the torque T_L [Nm] to speed ω [rpm] is represented by [11]:

$$G(s) = \frac{1}{sJ+B} \quad (5)$$

T_L [Nm]: load torque, ω [rpm]: achieved speed, ω_r [rpm]: reference speed, J [kgm^2]: moment of inertia, B [Pas]: coefficient of viscous force, α: speed control bandwidth [11].

$$F(s) = \frac{\alpha}{s}\left(\frac{1}{sJ+B}\right) \quad (6)$$

By transforming the previous equation, we get:

$$F(s) = \alpha J + \frac{\alpha B}{s} = K_p + \frac{K_i}{s} \quad (7)$$

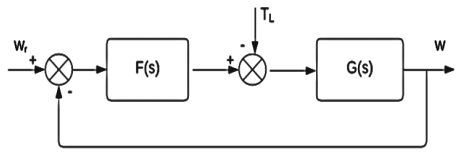

Figure 1
Simplified PMBLDC Dynamic Model [11]

In our previous research [11], the PI controller was used to control the simplified electric motor model, which considers the speed-torque envelope. However, for the EV application in this research, the PID was used to control the speed of the powertrain (e-Crafter) for both the advanced and simplified powertrains, adding the derivative part of the PID. Therefore, the mathematical model for the simplified model described in equations (5)-(7) represents only the general theoretical description of the motor controlled by the PI control. Figure 2 shows the motor design process configured with the three-phase inverter.

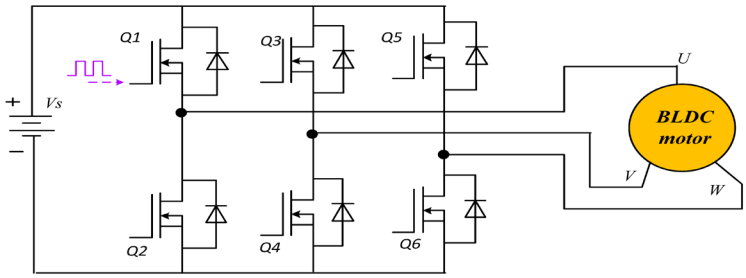

Figure 2
PMBLDC Motor Design [14]

3 Motor Advanced Control

This section presents the advanced control strategy known as trapezoidal or six-step commutation logic control of the three-phase motor suitable for the proposed EV application. The three-phase motor subsystem includes the power battery, DC-DC converter, electric motor, three-phase inverter and control blocks. This study used MOSFET transistors to simulate the DC-DC converter and the three-phase inverter. The battery source for the study was a 2011 Nissan Leaf Pack with a 360 V 24 kWh capacity. The research was conducted in comparison to a VW Crafter outfitted with a 2011 Nissan Leaf battery, which served as the cornerstone for our examination. Furthermore, this research compared the simulated energy consumption to real-world measurements as adapted data for validation purposes.

3.1 Hall Sensor

The use of Hall sensors to drive the PMBLDC motor's motion has progressed significantly as sensor technology and control methodologies have advanced. Hall sensors are commonly used to determine rotor position, allowing for precise motor commutation and control. Hall sensor-based control systems have advanced in sophistication and dependability [15, 16]. "In a typical low-cost drive, the voltage source inverter is controlled by the signals produced by three Hall effect sensors that are used to detect the rotor position" [16]. These sensors should be positioned precisely 120 electrical degrees apart [16]. Therefore, when the rotor is in motion, the Hall sensors accurately perceive the rotor position, allowing the controller to ascertain the precise stride of the motor. Using this data, the controller triggers the relevant stages following the predetermined order [30]. The active phases produce flux, resulting in the rotation of the rotor [30]. A six-step commutation guarantees a relatively smooth rotation of the PMBLDC motor by supplying voltage to the motor windings in a controlled sequence [30]. Tables 1 and 2 present the motor's forward and reverse switching sequences during the six-step commutation logic.

Table 1
Switching sequence of forward operation [11]

S/N	Switching Sequence					
	AH	AL	BH	BL	CH	CL
1	1	0	0	0	0	1
2	0	0	1	0	0	1
3	0	1	1	0	0	0
4	0	1	0	0	1	0
5	0	0	0	1	1	0
6	1	0	0	1	0	0

Table 2
Switching sequence of reverse operation [11]

S/N	Switching Sequence					
	AH	AL	BH	BL	CH	CL
1	0	1	0	0	1	0
2	1	0	0	0	0	1
3	0	0	1	0	0	1
4	0	0	0	1	1	0
5	1	0	0	1	0	0
6	0	1	1	0	0	0

Within the realm of PMBLDC motors, "quadrant operation" denotes the several modes of operation that arise from the interplay between motor speed and torque. The "torque-speed characteristic quadrants" are frequently used to describe the performance and features of the motors. There are four quadrants of operation [18].

Table 3
PMBLDC motor four-quadrant operation [18]

Quadrants	Quadrant Operations		
	Motor Operation Mode	Speed	Torque
1	Forward Accelerating Mode	Positive	Positive
2	Forward Braking Mode	Positive	Negative
3	Reverse Accelerating Mode	Negative	Negative
4	Reverse Braking Mode	Negative	Positive

The speed and torque are positive in the first quadrant, which is the vehicle's forward accelerating mode [18]. In this situation, the vehicle needs positive torque and speed to climb the hill. In the second quadrant, the vehicle is coming down the hill. In this situation, the vehicle requires the motor's positive speed and negative torque. At the same time, in the third quadrant operation, the vehicle can go uphill in the reverse direction, and both the speed and torque are negative. However, in the fourth quadrant, the speed is negative while the torque is positive; hence, the vehicle can come down the hill in the reverse direction.

4 Integration of the Motor

In this section, the simplified and advanced motor models are integrated into the vehicle model, forming the powertrain of the VW Crafter in different advancedity fashions. The simulated models implemented in this research using MATLAB/Simulink/Simscape are based on the real-world electric vehicle model of the University of Debrecen, shown in Figure 3. The reference vehicle is a hybrid operated independently in a pure electric or conventional hybrid mode.

Figure 3
VW Crafter Hybrid Vehicle

4.1 Advanced Powertrain Model

The advanced model of the PMBLDC motor was implemented as follows. First, a drive cycle input was used to enter the desired speed required for the motor. Then, to control the input voltage flowing into the system, a PID controller was

implemented to control the voltage source, using pulse width modulation (PWM) into the required quantity (duty cycle). Next, to get a final smooth modulated voltage, a DC-DC converter was used to ensure the smoothness and accuracy of the voltage amount. The next step is to convert the voltage into the three-phase inverter from a DC voltage to a three-phase voltage to supply the motor [30]. The system's main components are the PMBLDC motor, a rotor, and a stator. This makes the motor rotate, requiring three-phase voltage generated by the three-phase inverter by the principle of six-step commutation. A Hall effect sensor is inserted in the motor to detect the position of the rotor. This Hall effect sensor sends a feedback signal to the commutation logic matrix to energize the two specific phases at each step of the six steps of the motor rotation [30]. The advanced control strategy aims to maximize the angle between the stator and the rotor fields to produce the high torque required for efficient motor performance in EV applications. Figure 4 shows a detailed model of the three-phase motor integrated into the VW Crafter to run as a pure electric vehicle.

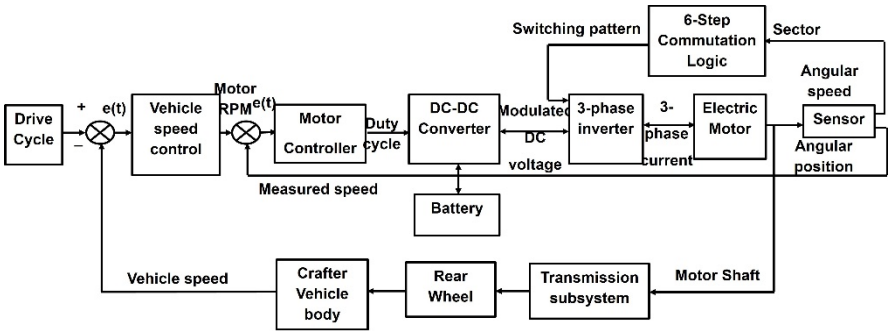

Figure 4
Advanced Powertrain Model [11]

4.2 Simplified Powertrain Model

This model is more straightforward than the advanced model of the PMBLDC motor. It contains only a PID controller, a PMBLDC motor, and a feedback sensor. The central part of this model is the PMBLDC motor, which is controlled by a PID controller that controls its operation and speed; the motor then sends a feedback signal by using the feedback sensor to the PID controller to compare the reference speed and the obtained speed as a closed loop system operation. This model uses two different feedback loops of control: an inner feedback loop to control the current flowing through and an outer feedback loop to control the speed of the motor. This model is supplied by all the sources (Vcc) and divided into three branch sources: Vref, Vdir, and Vbrk. The Vref is responsible for the forward rotation of the motor, while Vdir is for the reverse motion of the motor, and when Vbrk is

engaged, it cuts the flow of voltage from Vref and Vdir to force the motor to stop operating. The simplified modeling approach was adapted from [17, 19].

However, the operation design of this model is set as follows: First, the Vref is set to its higher value, which is 2 V, when the motor rotates in a forward direction with the speed of 40,000 rpm for one second. After that, the Vref is set to low, and the Vdir is set to high 2 V for one second, which converts the direction of the motor to the reverse direction with the speed of -40,000 rpm. Finally, after two seconds of operation, the Vbrk is energized to cut the power from Vref and Vdir to make the motor decelerate to 0 RPM [17]. The simplified level of the model aims to simplify the advancedity of the detailed model to optimize its performance and run faster. Figure 5 shows the simplified motor model integrated with the vehicle model, forming the VW Crafter in a simplified fashion.

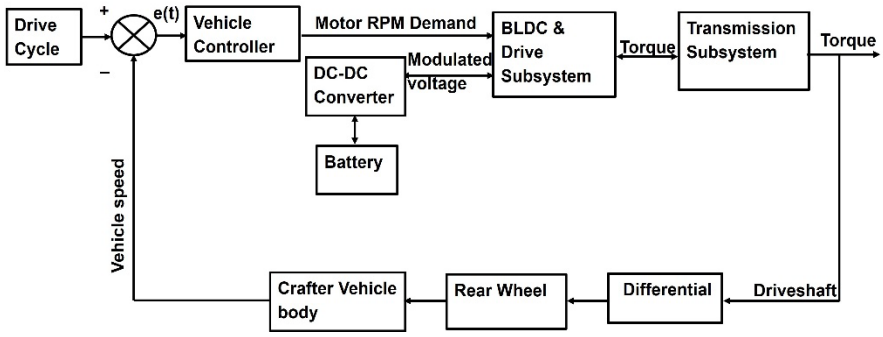

Figure 5
Simplified Powertrain Model [18]

4.3 Open-Loop and Close-Loop Models

In this section, a detailed analysis of the advanced powertrain is conducted. The model is analyzed on the basis of open-loop and closed-loop. The model of Figure 6 represents the open-loop advanced powertrain system presented in a simplified manner. This model contains the duty cycle input block for applying and adjusting the reference speed input, an advanced model of the PMBLDC motor explained above, a four-wheeler EV, and a transmission system (four-speed gearbox) to connect between the motor and the EV and transmit the rotation motion from the motor to the vehicle with different stages of speed.

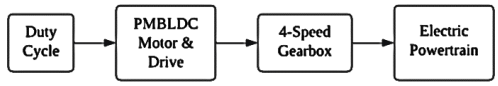

Figure 6
Open loop powertrain

The model of Figure 7 represents the closed-loop advanced powertrain system presented in a simplified manner. This model contains the drive cycle block for applying and adjusting the reference speed input, the vehicle, the transmission system, the advanced model of the PMBLDC motor and its drives such as the PID controller, DC-DC converter, the three-phase inverter, the pulse width modulation, the trapezoidal control strategy, and the sensor.

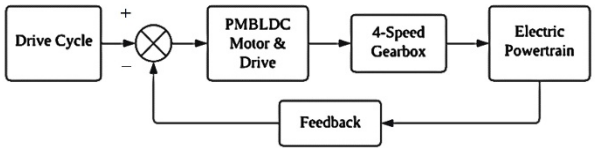

Figure 7
Close loop powertrain

The transmission system (four-speed gearbox) connects the motor and the electric vehicle, allowing the rotation motion to transmit from the motor to the wheel. This model has two feedback configurations: one is for the motor itself, and the other feedback is for the whole powertrain system. These feedback signals are sent into the input to compare the output speed with the reference input to fix any deviations. Since the PID controller regulating the vehicle can provide the torque demand to the powertrain, the two feedbacks were replaced with one feedback so that the PID controller regulates the vehicle speed and allocates optimal speed and torque to the motor for optimal energy consumption. The purpose of the open-loop model was to check the behavior of the powertrain on open-loop response and the need to optimize the closed-loop model. Table 4 presents the specifications used in the three-phase motor modeling.

Table 4
Motor main parameters [30]

S/N	Motor Parameters		
	Parameters	Values	Units
1	Connection	Y-Connection	
2	Number of poles	4-Poles	
3	Back EMF profile	Perfect trapezoid	[V]
4	Inductance of Stator d-axis (Ld)	0.0001	[H]
5	Inductance of Stator q-axis (Lq)	0.0001	[H]
6	Inductance of Stator Zero Sequence (L0)	0.00016	[H]
7	Stator resistance per phase (Rs)	0.001	[Ohm]
8	Flux Linkage	0.18	[Weber]
9	Rotor damping	0.1	[Nm/(rad/s)]
10	Rotor Inertia	0	[kgm^2]
11	Ambient temperature	298.15	[K]

5 Optimal Solutions

5.1 Manual Tuning

Two methods of tuning the PID controller were used in this research. Manual and GA techniques. The gain parameters such as proportional gain (K_p), integral gain (K_i), and derivative gain (K_d) were adjusted manually to achieve minimal deviation, resulting in better performance and system stability. The manual tuning of the PID parameters did not yield a satisfactory performance due to the inherent nonlinearities present in the system. Therefore, the GA was ued to search for the optimal gains of the PID parameters.

5.2 Genetic Algorithm

A Genetic algorithm is inspired by the process of natural selection. The GA allows the evolution of possible solutions to advanced computational problems. This research uses it to find the best gain values of the PID controller for the advanced model of the closed loop powertrain to gain the least minimum error values during the process. Therefore, PID parameters (K_p, K_i, K_d) were obtained optimally using the GA optimization technique based on performance criteria such as integral absolute error (IAE), integral square error (ISE), integral time absolute error (ITAE), and integral time square error (ITSE) were introduced in this research to fine-tune the evaluation process. The optimization problems are applied in technical and non-technical fields to find the optimal point of the objective function [20, 21]. Specifically, the optimization problem in vehicle engineering is maximizing the system's efficiency and reducing energy consumption and emissions [22]. From the research perspective, other optimization techniques have been adopted to tune the gains of the PID controller, such as fuzzy logic (fuzzy-PI), as in [23, 24], and an extended symmetrical optimum method, as in [25]. However, the GA technique inspired by natural evaluation [26] has been commonly applied to optimization problems, such as in [27, 28], due to its simplicity and faster convergence, and it can be used for multi-objective optimization problems. Figure 8 shows GA's implementation of the PID controller for the system. The reference represents the desired or controlled vehicle speed; the error is the difference between the actual speed (output) and the desired speed (reference). Based on the objective function, the optimal values of the controller gains are computed and fed to the PID controller for the efficient performance of the powertrain (plant).

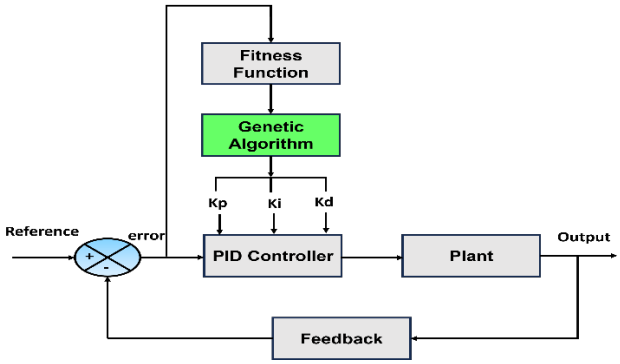

Figure 8
GA-PID Structure [29]

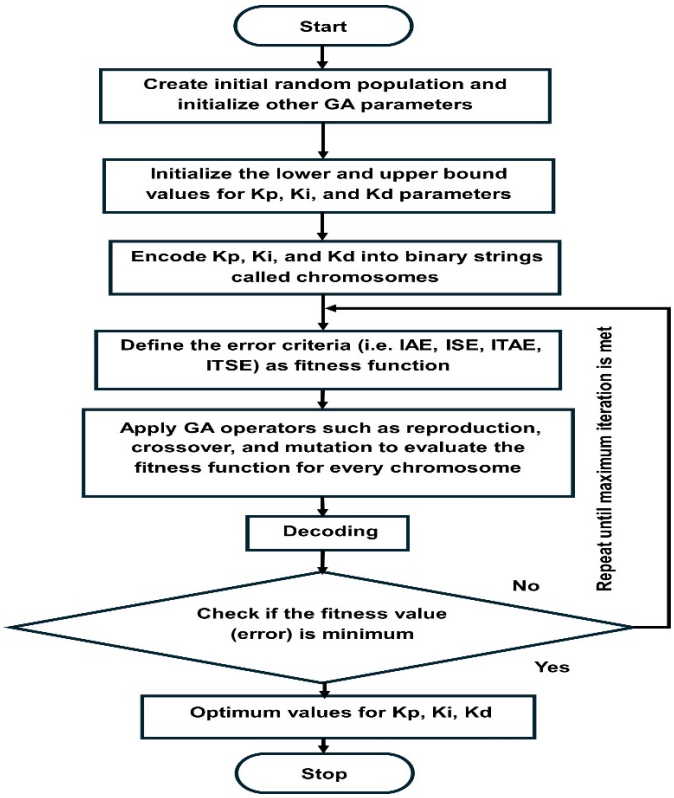

Figure 9
GA Flowchart [29]

Figure 9 shows a flowchart of the GA used to obtain the optimal gains of the PID controller on the basis of the integral cost functions. The optimization problem, which is based on achieving optimal speed tracking, is defined in terms of the PID performance assessment criteria, such as the IAE, ISE, ITAE, and ITSE. These errors should be minimum if the maximum iteration is met. The following equations are used to represent the objective function as expressed in [29] mathematically as follows:

$$\begin{cases} IAE = \int_0^\infty |e(t)|dt \\ ISE = \int_0^\infty |e(t)|^2 dt \\ ITAE = \int_0^\infty t|e(t)|dt \\ ITSE = \int_0^\infty t|e(t)|^2 dt \end{cases} \tag{8}$$

Therefore, the proposed optimization algorithm was applied to refine a population parameter setting using the GA operators until the maximum iteration that represents minimum value of the integral errors was met and the optimal gains of the controller were found. In this optimization problem, the reference refers to the desired vehicle speed, which stands as the input for the PID controller (Figure 8). The error signal was fed to the PID controller to regulate the vehicle's speed. Hence, the controller provides the required motor speed to produce the optimal torque for electric vehicle applications. The system model consists of the battery, electric drive system (motor and power electronics), vehicle, and controller, which were integrated into an optimization framework based on the GA optimization technique to optimize performance. Table 5 presents the GA parameters used for the optimization problem.

Table 5
Genetic Algorithm Parameters

S/N	Parameters	Values
1	Selection Strategy	Random
2	Fitness Peformance	Proportional
3	Generations	10
4	Population Size	20
5	Number of Variables	3
6	Lower Bound (LB)	[0 0 0]
7	Upper Bound (UB)	[200 200 200]

6 Results

6.1 Simulation Results

Table 6 presents the fitness values of the optimal PID parameters obtained using the manual and GA optimization methods. It was observed that during the manual tuning, when the K_d was greater than K_i and K_p, the output errors were at their maximum. The minimum error values were obtained when the K_p was gradually greater than K_d and K_i, and so on. Therefore, tuning the controller using the manual tuning technique is challenging. However, the minimum value of errors was obtained by applying the genetic algorithm technique. This proves the effectiveness and accuracy of the GA technique.

Table 6
GA and manual tuning-based performance evaluation comparison

Tuning Method	Controller Gains			Fitness Values			
	K_p	K_i	K_d	ISE	ITSE	IAE	ITAE
GA-PID	181.442	23.5353	61.597	1.594	0.4528	1.365	3.832
Manual	100	150	200	5.369	14.94	7.347	52.01

The following figures present the simulation results of the different models implemented by MATLAB/Simulink. The advanced model simulation results represent the speed and temperature relationship and the comparison between the actual speed and the desired speed graphs. For the simplified model, the results show the variation between the desired speed and the obtained speed, and they also show the effect of ambient temperature on the motor temperature. The results of the open- and closed-loop powertrain models show the speed graphs and how gear modification affects the speed. The method used in MATLAB for modeling in this paper was adapted from [30, 31].

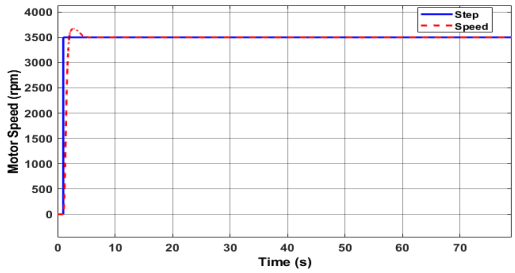

Figure 9
Advanced Motor Model Speed due to a step input

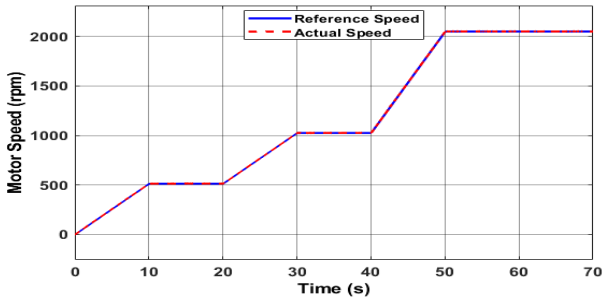

Figure 10
Advanced Motor Model due to input speed ranges [30]

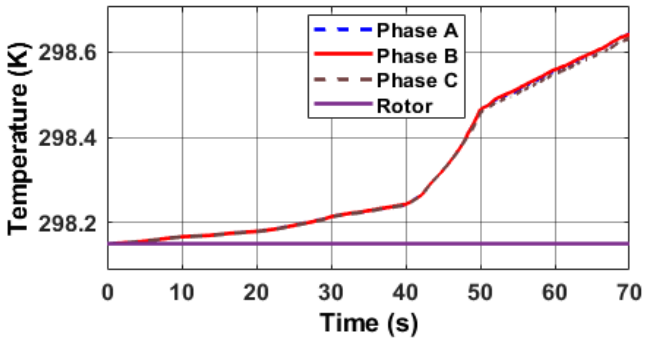

Figure 11
Temperature Of The Rotor And The Phases

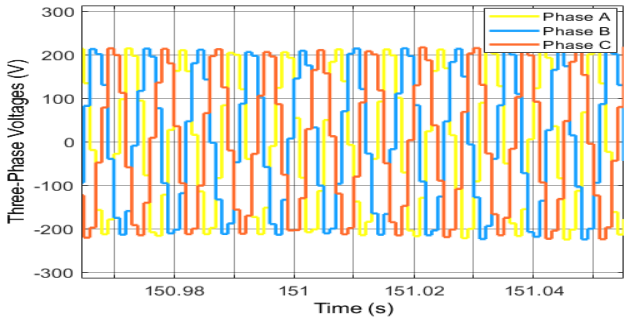

Figure 12
Advanced Powertrain Three-Phase Voltages

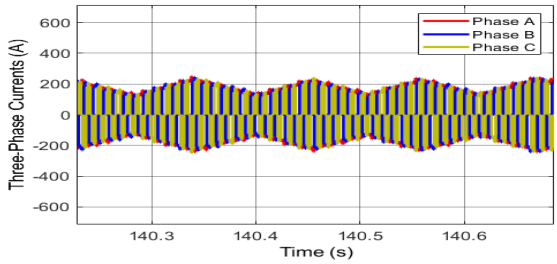

Figure 13
Advanced powertrain Three-Phase Currents

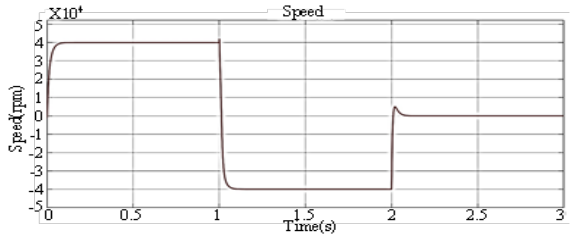

Figure 14
Simplified Motor Model Speed adapted from [17]

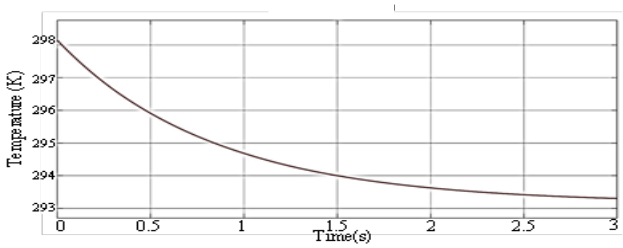

Figure 25
Simplified Motor Model T , rature adapted from [19]

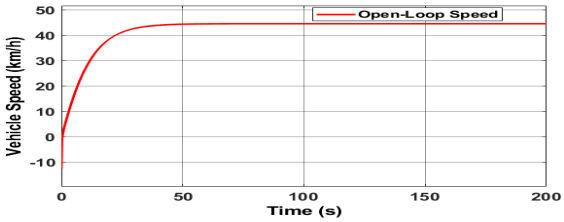

Figure 16
Vehicle Open Loop Speed

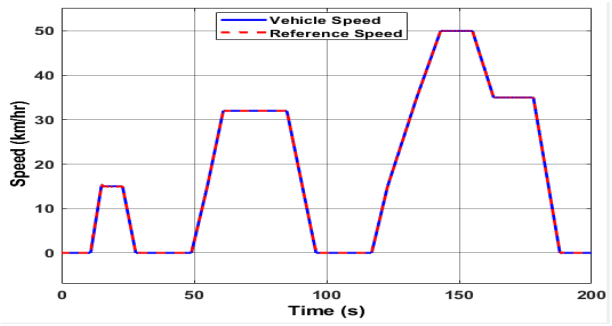

Figure 17
Advanced Model Vehicle Speed

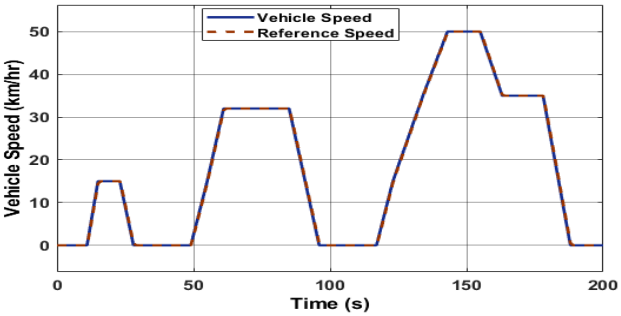

Figure 18
Simplified Model Vehicle Speed

6.2 Optimal Energy Consumption

Figure 19 shows the energy consumption of the VW e-Crafter-based 2011 Nissan Leaf traction battery pack of 24 kWh rated capacity and 360 V nominal voltage PMBLDC traction motor expressed in kWh/1 km distance travelled. Table 7 presents the energy consumption per 100 km of the distance travelled by the vehicle, and Table 8 presents the real measurement of different versions of the vehicle, which was calculated based on the 2011 Nissan Leaf for validation purposes.

Table 7
VW e-Crafter Simulated Energy Consumption based PMBLDC Motor

Controller Gains			Simplified Powertrain
K_p	K_i	K_d	Energy Consumed [kWh/100 km]
100	200	50	17.34
100	500	0	17.42

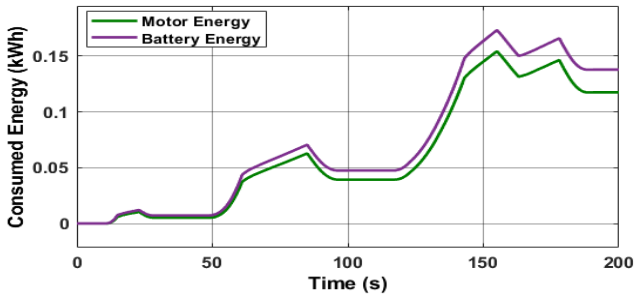

Figure 19
Energy Consumption per 1 km

Table 8
Meaured Energy consumption results [11]

Vehicle Model and Year Manufactured	Energy consumed [kWh/100km]
VW crafter 2020	19.51
VW crafter 2019	14.74
VW crafter 2018	14.99

7 Discussion

The results are discussed as follows: Figure 9 shows the motor speed when tested with a step input at 3500 rpm. Figure 10 shows the speed graph of the advanced model of the permanent magnet brushless DC motor as adapted from [30]. It shows that the motor was accelerating, representing the gradual increase in speed from 0 rpm to its maximum value of 2000 rpm. Figure 11 shows the temperature graph of the PMBLDC motor, including the rotor temperature and the temperature of the coil windings in the stator. It indicates a gradual, stable increase in the winnings temperature from the initial temperature (ambient temperature) of the whole motor, which is 25 degrees Celsius, to a maximum temperature of 25.4 degrees Celsius. The temperature increased gradually as the motor accelerated, and the speed increased until it reached the peak speed, which shows the stability of the motor system. Figure 12 shows the graph of the main characteristic of the PMBLDC motor for the advanced powertrain, which is the trapezoidal three-phase voltage. This result indicates the trapezoidal three-phase voltage supplied by the three-phase inverter. Figure 13 shows the three-phase current graph obtained from the three-phase inverter for energizing the motor for the advanced powertrain. Figure 14 shows the 3-second operation of the simplified model of the PMBLDC motor. This operation can be divided into three steps: two steps of rotation and one step of braking.

Firstly, the system operates at a positive forward constant speed for one second, and then the motor changes its direction into a reverse motion for one second. Finally, the voltage cuts off, and the mortar stops operating. A thermal model was implemented in the simplified model to study the effect of the ambient temperature on the motor. The ambient temperature was set to 10 degrees Celsius. In contrast, the initial temperature of the motor was set at 24.5 degrees Celsius. A cooling system and heat exchanger were implemented to preserve the system's stability by reducing the motor's temperature. This reduced the motor temperature from 24.5 degrees Celsius to 20 degrees Celsius, as shown in Figure 15.

The open loop powertrain speed is shown in Figure 16. This system is an open-loop system with a duty cycle input. The duty cycle input is set to 0.85. The Figure shows a stable increase in speed, reaching the maximum value and continuing at a constant speed, indicating a stable system. The powertrain was modeled based on four gearahift. The gear was set to a different level every 15 seconds. The gear was in neutral mode for the first period, which showed zero speed change. As the gear changed from first to fourth gear, the speed increased while the torque decreased. In the last period, reverse gear was applied, the speed dropped to the negative side. Figures 17 and 18 show the desired speed from the drive cycle input block of the advanced and simplified powertrain models based on the new European drive cycle (NEDC). The aim was to compare the desired speed input and the actual speed of the powertrain. The proposed PID controller, tuned based on the GA technique, was used to ensure optimal energy consumption for the e-Crafter. One of the sufficient methods to measure system stability is to compare the desired speed input and the obtained speed output. Therefore, the vehicle's actual speed has successfully followed the reference speed.

The proposed electrical machine is quite promising for EV application, as shown in Figure 19 and presented in Table 7. The battery and motor energy consumption were 17.42 kWh/100 km and 15.49 kWh/100 km, respectively. According to Table 7, these values change when there is a change in the driver's behavior. However, the power consumption for the battery and the motor were 26.03 kW and 23.66 kW, respectively. Therefore, based on these, the energy and power efficiencies for the simplified model motor were 89.92% and 90.90%. It can be observed that the simplified model of the motor in the EV performed excellent in both the energy and power aspects. This shows less energy loss over the operation cycle of the proposed motor in e-Crafter.

Moreover, according to Tables 7 and 8, the measured and simulated energy consumption for the VW Crafter was 19.51 kWh/100 km and 17.34 kWh/100 km, respectively. This shows an 11.12% decrease in the energy consumption for the 2020 manufactured VW e-Crafter on the basis of the 2011 Nissan Leaf traction battery. However, although the GA-PID is quite promising in optimal speed tracking for advanced and simplified models, further redesign is needed to ensure the advanced model's accuracy. Due to inaccurate parameter estimation and other factors, the advanced model did not perform well in some performance criteria, such

as battery power and energy, drawing high currents that led to high recovery energy during deceleration. Therefore, considering this limitation, further study will enhance the advanced model of the motor and rebuild on the results presented in our previous studies, as reported in [11], ensuring its accurate performance over its entire cycle of operation.

Conclusion

In conclusion, this research has presented the development of an enhanced PID controller tuned using GA on the basis of integral error objective functions. Therefore, the optimization process of the e-Crafter powertrain-based PMBLDC electrical machine has achieved promising results with an 11.12% decrease in energy consumption. The proposed controller has successfully tracked the reference and the actual speeds for both the simplified and advanced models, presenting a stable system. Implementing the ambient temperature model in the simplified motor model resulted in more realistic outcomes while applying a cooling system and heat exchanger helped decrease overall motor temperature. By using thermal measurement sensors in the advanced model of the vehicle, it can be seen that the temperature rises gradually as the speed does, with no variations. The proposed electrical machine is quite promising in electric vehicles, demonstrating efficient performance. Future studies will propose an extended symmetrical optimum method to ensure a convenient tuning because it ensures a compromise to a set of the proposed performance indices imposed on the e-Crafter powertrain control system and guarantees their achievements. Secondly, the parameters of the advanced model will be measured using hardware-in-the-loop (HIL) to ensure the motor is operating in all its cycles of operation for the EV application. Finally, the TIE-GA technique can be applied to optimize the PID controller to enhance the performance of the advanced motor model, suppress noises, and improve robustness in its design.

Acknowledgement

This work was supported by the TKP2020-NKA-04 project implemented with support from Hungary's National Research, Development, and Innovation Fund, financed under the 2020-4.1.1-TKP2020 funding scheme. The authors wish to thank the Hungarian Research Fund (OTKA K143595).

References

[1] Yong, J. Y., Ramachandaramurthy, V. K., Tan, K. M., & Mithulananthan, N. (2015) A review on the state-of-the-art technologies of electric vehicle, its impacts and prospects, Renewable and Sustainable Energy Reviews, Vol. 49, pp. 365-385, https://doi.org/10.1016/j.rser.2015.04.130

[2] Zainuri, F., Danardono A. S, D. A., Adhitya, M., Subarkah, R., Filzi, R., Rahmiati, T., … Ridwan (2024) Analytical Conversion of Conventional Car to Electric Vehicle Using 5KW BLDC Electric Motor. Jurnal Penelitian

Pendidikan IPA, Vol. 10, No. 9, pp. 6703-6708, https://doi.org/10.29303/jppipa.v10i9.8599

[3] Kim, SC., Sangam, N., Pagidipala, S., Salkuti, S. R. (2022) Design and Analysis of BLDC Motor Driver for Hybrid Electric Vehicles. In: Salkuti, S. R., Ray, P. (eds) Next Generation Smart Grids: Modeling, Control and Optimization. Lecture Notes in Electrical Engineering, Vol. 824, pp. 297-311, Springer, Singapore, https://doi.org/10.1007/978-981-16-7794-6_12

[4] Subbarao, M., Dasari, K., Duvvuri, S. S., Prasad, K. R. K. V., Narendra, B. K., & Krishna, V. M. (2024) Design, control and performance comparison of PI and ANFIS controllers for BLDC motor driven electric vehicles. Measurement: Sensors, Vol. 31, 101001, https://doi.org/10.1016/j.measen.2023.101001

[5] Sayed, K., El-Zohri, H. H., Ahmed, A., & Khamies, M. (2024) Application of Tilt Integral Derivative for Efficient Speed Control and Operation of BLDC Motor Drive for Electric Vehicles. Fractal and Fractional, Vol. 8, No. 1, 61, https://doi.org/10.3390/fractalfract801006

[6] Krishnan, D., Mythili, R., Kiruthickroshan, V., Roopha, V., Sudhakar, M., & Deepak, M. (2024, April) Optimized Design and Deployment of BLDC Motor Poles in E-Vehicle. In 2024 International Conference on Science Technology Engineering and Management (ICSTEM) (pp. 1-4) IEEE, https://doi.org/10.1109/ICSTEM61137.2024.10561152

[7] Sandeep, V., & Shastri, S. (2019) Analysis and design of PMBLDC motor for three wheeler electric vehicle application. In E3S web of conferences (Vol. 87, p. 01022) EDP Sciences, https://doi.org/10.1051/e3sconf/20198701022

[8] Naqvi, S. S. A., Jamil, H., Iqbal, N., Khan, S., Lee, D. I., Park, Y. C., & Kim, D. H. (2024) Multi-objective optimization of PI controller for BLDC motor speed control and energy saving in Electric Vehicles: a constrained swarm-based approach. Energy Reports, 12, 402-417, https://doi.org/10.1016/j.egyr.2024.06.019

[9] Long, B., Lim, S. T., Ryu, J. H., & Chong, K. T. (2013) Energy-regenerative braking control of electric vehicles using three-phase brushless direct-current motors. Energies, Vol. 7, No. 1, pp. 99-114, https://doi.org/10.3390/en7010099

[10] Nandakumar, M. (2024) Design of BLDC motor drive system using alternative controllers for performance evaluation in electric vehicle applications. International Journal of Vehicle Design, Vol. 94, No. 1-2, pp. 57-82, https://doi.org/10.1504/IJVD.2024.136234

[11] Babangida, A., & Szemes, P. T. (2022, September) Energy consumption simulation and economic benefit analysis for a light duty urban commercial electric vehicle. In 2022 IEEE 20th International Power Electronics and

Motion Control Conference (PEMC) (pp. 667-672) IEEE, https://doi.org/10.1109/PEMC51159.2022.9962881

[12] Ajmal, A. M., & Ramachandaramurthy, V. K. (2015) Regenerative Braking of Electric Vehicle with Brushless DC Motor. Applied Mechanics and Materials, Vol. 785, pp. 280-284, https://doi.org/10.4028/www.scientific.net/AMM.785.280

[13] Ansari, U., & Alam, S. (2011, March) Modeling and control of three phase BLDC motor using PID with genetic algorithm. In 2011 UkSim 13th international conference on computer modelling and simulation (pp. 189-194) IEEE, https://doi.org/10.1109/UKSIM.2011.44

[14] Sayed, K., El-Zohri, H. H., Ahmed, A., & Khamies, M. (2024) Application of Tilt Integral Derivative for Efficient Speed Control and Operation of BLDC Motor Drive for Electric Vehicles. Fractal and Fractional, Vol. 8, No. 1, 61

[15] Trivedi, M. S., & Keshri, R. K. (2020) Evaluation of predictive current control techniques for PM BLDC motor in stationary plane. IEEE Access, Vol. 8, pp. 46217-46228, https://doi.org/10.1109/ACCESS.2020.2978695

[16] Alaeinovin, P., Chiniforoosh, S., & Jatskevich, J. (2008, October) Evaluating misalignment of hall sensors in brushless DC motors. In 2008 IEEE Canada Electric Power Conference (pp. 1-6) IEEE, https://doi.org/10.1109/EPC.2008.4763350

[17] Brushless DC Motor - MATLAB & Simulink. Accessed: Nov. 25, 2023, Available: https://www.mathworks.com/help/sps/ug/brushless-dc-motor.html

[18] Babangida, A., & Szemes, P. T. (2024) Dynamic Modeling and Control Strategy Optimization of a Volkswagen Crafter Hybrid Electrified Powertrain. Energies, Vol. 17, No. 18, 4721, https://doi.org/10.3390/en17184721

[19] Electric Vehicle Configured for HIL - MATLAB & Simulink. Accessed: Nov. 25, 2023, Available: https://www.mathworks.com/help/sps/ug/electric-vehicle-configured-for-hil.html

[20] Precup, R. E., Hedrea, E. L., Roman, R. C., Petriu, E. M., Szedlak-Stinean, A. I., & Bojan-Dragos, C. A. (2020) Experiment-based approach to teach optimization techniques. IEEE Transactions on Education, Vol. 64, No. 2, pp. 88-94, https://doi.org/10.1109/TE.2020.3008878

[21] Ibrahim, S. K., Rad, M. M., & Fischer, S. (2023) Optimal Elasto-Plastic Analysis of Reinforced Concrete Structures under Residual Plastic Deformation Limitations. Acta Polytechnica Hungarica, Vol. 20, No. 1

[22] Milovančević, M., Milčić, D., Andjelkovic, B., & Vračar, L. (2022) Train Driving Parameters Optimization to Maximize Efficiency and Fuel Consumption. Acta Polytechnica Hungarica, Vol. 19, No. 3, pp. 143-154

[23] Precup, R. E., Preitl, S., & Korondi, P. (2007) Fuzzy controllers with maximum sensitivity for servosystems. IEEE Transactions on Industrial Electronics, Vol. 54, No. 3, pp. 1298-1310, https://doi.org/10.1109/TIE.2007.893053

[24] Roman, R. C., Precup, R. E., & David, R. C. (2018) Second order intelligent proportional-integral fuzzy control of twin rotor aerodynamic systems. Procedia computer science, Vol. 139, pp. 372-380, https://doi.org/10.1016/j.procs.2018.10.277

[25] Preitl, S., & Precup, R. E. (1996) On the algorithmic design of a class of control systems based on providing the symmetry of open-loop Bode plots. Scientific Bulletin of UPT, Transactions on Automatic Control and Computer Science, Vol. 41, No. 55, pp. 47-55

[26] Menich, P., & Kopják, J. (2023) Optimal fuzzy controller, using a genetic algorithm for a ball on wheel system. Acta Polytechnica Hungarica, Vol. 20, No. 6, pp. 61-77

[27] Kilic, U., Essiz, E. S., & Keles, M. K. (2023) Binary anarchic society optimization for feature selection. Romanian Journal of Information Science and Technology, Vol. 26, No. 3-4, pp. 351-364

[28] Chopra, V., Singla, S. K., & Dewan, L. (2014) Comparative analysis of tuning a PID controller using intelligent methods. Acta Polytechnica Hungarica, Vol. 11, No. 8, pp. 235-249

[29] Nishat, M. M., Faisal, F., Evan, A. J., Rahaman, M. M., Sifat, M. S., & Rabbi, H. F. (2020) Development of genetic algorithm (ga) based optimized PID controller for stability analysis of DC-DC buck converter. Journal of Power and Energy Engineering, Vol. 8, No. 09, p. 8

[30] Design of Motor Controllers with Simscape. Available: https://github.com/mathworks/Design-motor-controllers-with-Simscape-Electrical (Accessed on November 10, 2023)

[31] Mathwork Electric All Terrain Vehicle. Available: https://github.com/mathworks/electric-all-terrain-vehicle?s_eid=PSM_15028 (Accessed on November 10, 2023)